21st Australasian Fluid Mechanics Conference
Adelaide, Australia
10-13 December 2018

RANS based CFD Prediction of Submarine Hydrodynamic Loads

D.A. Pook[1], D.B. Clarke[2a], M. Jones[2b], H. Quick[2b], D. Ranmuthugala[3,2a]

[1]Aerospace Engineering & Aviation
RMIT University, Bundoora, Victoria, 3083, Australia

[2a]Maritime Division, [2b]Air Division
Defence Science & Technology Group, Fishermans Bend, Victoria, 3207, Australia

[3]Australian Maritime College
University of Tasmania, Newnham, Tasmania, 7248, Australia

Abstract

The loads on a model-scale BB2 generic submarine geometry at angles of drift are predicted with Reynolds Averaged Navier Stokes (RANS) based Computational Fluid Dynamics (CFD) and compared against a wind tunnel experiment. Agreement between experiment and all RANS turbulence models was good for drift angles less than 10°. Appendage stall prediction varied with turbulence model used. The Baseline Reynolds Stress Model (BSL-RSM), favoured in literature for submarine load prediction, did not produce better agreement with the experiment. For an unappended BB2 model, the BSL-RSM model predicted loads in closer agreement with the experiment.

Introduction

Previous Reynolds Averaged Navier Stokes (RANS) based predictions of submarine loads often focus on axisymmetric geometries such as the unappended SUBOFF geometry (see [8] for a summary). Loads on an unappended submarine are significantly affected by the hull's leeward, open-separation that develops with incidence, a challenge for RANS models to predict accurately [11]. Due to the separation, the baseline Reynolds Stress Model (BSL-RSM) is found to more accurately predict loads when compared with two-equation models based on turbulent kinetic energy (k) and its dissipation (ε) or specific dissipation (ω) [6, 8, 11, 12].

For an appended submarine, Bettle [1] has compared RANS based load predictions for the Defence Research and Development Canada (DRDC) Standard Submarine (SS) against experiment [13] . For angles of drift, the BSL-RSM model was not found to significantly improve load prediction compared to the SST $k\omega$ model, the only other model evaluated. The exception was the prediction of the heave force and pitching moment when the drift angle exceeded 15°. At these drift angles, the BSL-RSM prediction was in better agreement with experiment. At an angle of drift, the sail tip vortex will create circulation around the hull, generating a heave force and pitching moment [2]. Failure of a turbulence model and/or grid to predict the sail wake circulation would result in incorrect out-of-plane loads.

To confirm the findings of [1], the loads of the BB2 generic submarine geometry [10, 9] will be predicted with RANS and compared against experiment. To improve fidelity, Computational Fluid Dynamics (CFD) modeling will include the wind tunnel walls and model mounting. Results for the unappended BB2 hull (axisymmetric) will also be presented, demonstrating the modeling is consistent with previously reported literature.

Experimental Details & Coordinate System

The BB2 submarine geometry is a generalised representation of a diesel-electric submarine (CAD available [10, 9]). Compared to the SUBOFF and the DRDC SS, the BB2 features a topside hull-casing (i.e. non-axisymmetric hull), X-plane aft-control-surfaces (ACS), and sail mounted hydroplanes.

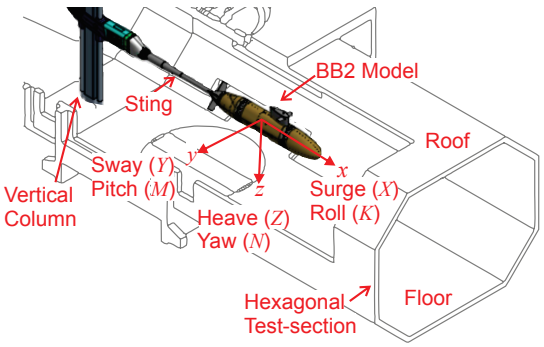

Figure 1: BB2 model in the DST LSWT with the body-fixed axis system. Model was rolled 90° and moved in the floor–roof plane to create a drift angle. Figure adapted from [7].

The scaled BB2 geometry, non-truncated model length (L) of 2 m, was tested in the Defence Science & Technology Group (DST) Low Speed Wind Tunnel (LSWT). Details of the experiment and complete measurements can be found in [7]. Figure 1 depicts the setup in the LSWT. The BB2 model was truncated at the stern ($x/L = -0.45$) and placed on an aft-mounted, 52 mm diameter sting, then positioned approximately 1.2 m upstream of a vertical column. Loads were measured with a 6-component internal strain gauge located amidships. Loads were reported in a body fixed axis system, origin amidships, as shown in figure 1.

The hull boundary layer was tripped at 5% of L. Appendages were untripped. The Reynolds number based on the non-truncated model length was 8×10^6. The freestream Mach number was 0.17, effectively incompressible flow. The casing and appendages of the BB2 model were removed to create an unappended (axisymmetric) model.

CFD Details

Grid

The CFD domain had two multi-block structured grid regions. The outer region boundaries were shaped to match the DST LSWT, 2.74 m × 2.13 m hexagonal test-section (see [4] for geometry), to account for blockage effects. An interface boundary condition joined it to a rectangular inner grid containing the BB2 geometry. Drift angles were produced by rotating the outer grid (LWST boundaries) while keeping the inner grid fixed, hence maintaining grid quality near the BB2 geometry.

Figure 2 shows the BB2 surface grid topology and the portion of the sting mounting included in the CFD. The remainder of

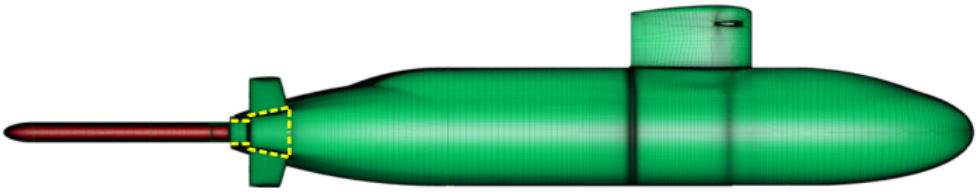

Figure 2: Appended BB2 CFD surface grid. Included sting shown in red. Included cavity shown with dashed yellow line.

Grid Number	Avg. y^+	Cell Count (million)
1	0.4	120
2	0.5	61.6
3	0.6	29.2
4	0.8	14.1

Table 1: Appended BB2 CFD grid details.

the sting and column was omitted. The BB2 wind tunnel model contained a large cavity to accommodate the sting. As shown in figure 2, only the opening region of the cavity was included in the CFD grid as the internal pressure should be constant away from the cavity entrance, hence not affect the loads.

Four grid refinements were created to assess numerical uncertainty. The cell count and the approximate y^+ are listed in table 1. All results to be reported use the finest grid (Grid 1). An unappended BB2 grid was created from the appended Grid 1. The total cell count of the unappended grid was 90.2 million.

RANS Turbulence Models

RANS turbulence closure models for evaluation were chosen based on reported past performance for submarine-like geometries. The following models were evaluated: SST $k\omega$, SST $k\omega$ with curvature correction (CC), BSL-RSM, $k\varepsilon$ Realizable, $k\varepsilon$ Realizable with curvature correction. The $k\varepsilon$ models used the enhanced wall treatment option in ANSYS Fluent. The ANSYS Fluent implementation of curvature correction allows a scaling factor. The ANSYS Fluent default value of 1.0 was used.

CFD Solver, Settings & Boundary Conditions

The RANS equations were solved with the Ansys Fluent version 18.1, incompressible, pressure-based solver. Pressure terms were differenced with the 2nd order scheme while momentum terms used the 3rd order MUSCL scheme. Turbulence terms used 2nd order differencing, except for the BSL-RSM Reynolds stresses that used 1st order as recommended by [5]. Gradients were evaluated with the Green-Gauss-cell-based method with the differentiable cell-to-face gradient limiter. The SIMPLEC algorithm was used for pressure-velocity coupling.

Non-slip walls were used for all model surfaces. Tunnel boundaries were set as non-slip walls to minimise cell count while still providing a blockage effect. A uniform velocity inlet was located $3.2L$ upstream of the model. An outflow boundary condition was placed $3.7L$ downstream of the model. All solutions were initialized with a uniform flow equal to the inflow.

Results

BB2 Appended Body

The appended BB2 loads are shown in figure 3. The three force (X' surge, Y'sway, Z' heave) and moment (K' roll, M' pitching, N' yaw) load coefficients are non-dimensionalised with $0.5\rho U^2L^2$ and $0.5\rho U^2L^3$ respectively. The magnitude of experimental loads are shown for positive ($+\beta$) and negative ($-\beta$) drift angles, with uncertainty estimates for the load cell. The large uncertainty estimate for surge is comparable to [13] for the DRDC SS (see [1]). RANS loads are computed for drift angles from 0° to 16°, in 2° increments. Numerical uncertainty is assessed at 0° and 10° drift using the method of [3].

From figure 3(a), (c), (e), there is a clear discontinuity in the measured surge, heave and pitching loads at an approximate drift angle of 14°. This indicates stall of one or more appendages. The exact stall angle differs slightly with the drift angle direction. The discontinuous increase of yaw moment post stall in figure 3(f) indicates an ACS stall (not sail). Combined with the discontinuous reduction of heave and pitching moment in figures 3(c) and (e), it indicates either the lower-windward or upper-leeward ACS has stalled. Considering the discontinuous increase in roll magnitude post stall in figure 3(d), it can be deduced that the ACS producing opposite roll to the sail has stalled, i.e the lower-windward ACS.

In an ideal experiment, load magnitudes should not vary with drift angle direction. Figure 3 shows the loads do not vary significantly with drift angle direction prior to stall. The exception is the pitching moment which will be discussed later.

The RANS predicted loads, shown in figure 3, are generally within experimental uncertainty bounds to at least 10° drift, except for the pitching moment to be discussed later. At 10° drift, the numerical uncertainty bounds overlap (excluding the pitching moment), preventing any conclusion about the models predicting different loads up to this drift angle.

For drift angles beyond 10°, significant differences in the loads are apparent with turbulence model. The discontinuities in the BSL-RSM model loads at 12° drift indicates appendage stall. This is a significantly lower drift angle than the SST $k\omega$ and $k\varepsilon$ Realizable models that exhibit stall at 14°, experiment at approximately 14°, and the curvature correction models that do not exhibit stall in the computed range. The RSM-BSL stall is also different, with large changes in surge, sway and roll loads beyond a drift angle of 14°. Examination of individual appendage loads (not shown) reveals the BSL-RSM model is predicting stall of the lower-windward ACS first, followed by stall of the sail. No other models, nor experiment, show evidence of the sail stalling within the examined drift angle range.

For drift angles below 10°, only the pitching moment in figure 3(e) shows significant variation with turbulence model. Interestingly, the SST $k\omega$ models follow the experimental positive drift angle results while the remaining turbulence models follow the negative drift angle results.

Axisymmetric Body

For the unappended BB2 hull, the BSL-RSM model can be seen in figure 4 to predict loads in better agreement with experiment. The curvature correction of the SST $k\omega$ model improves the prediction of the sway force and yaw moment slightly compared to the standard SST $k\omega$ model. The difference between SST $k\omega$

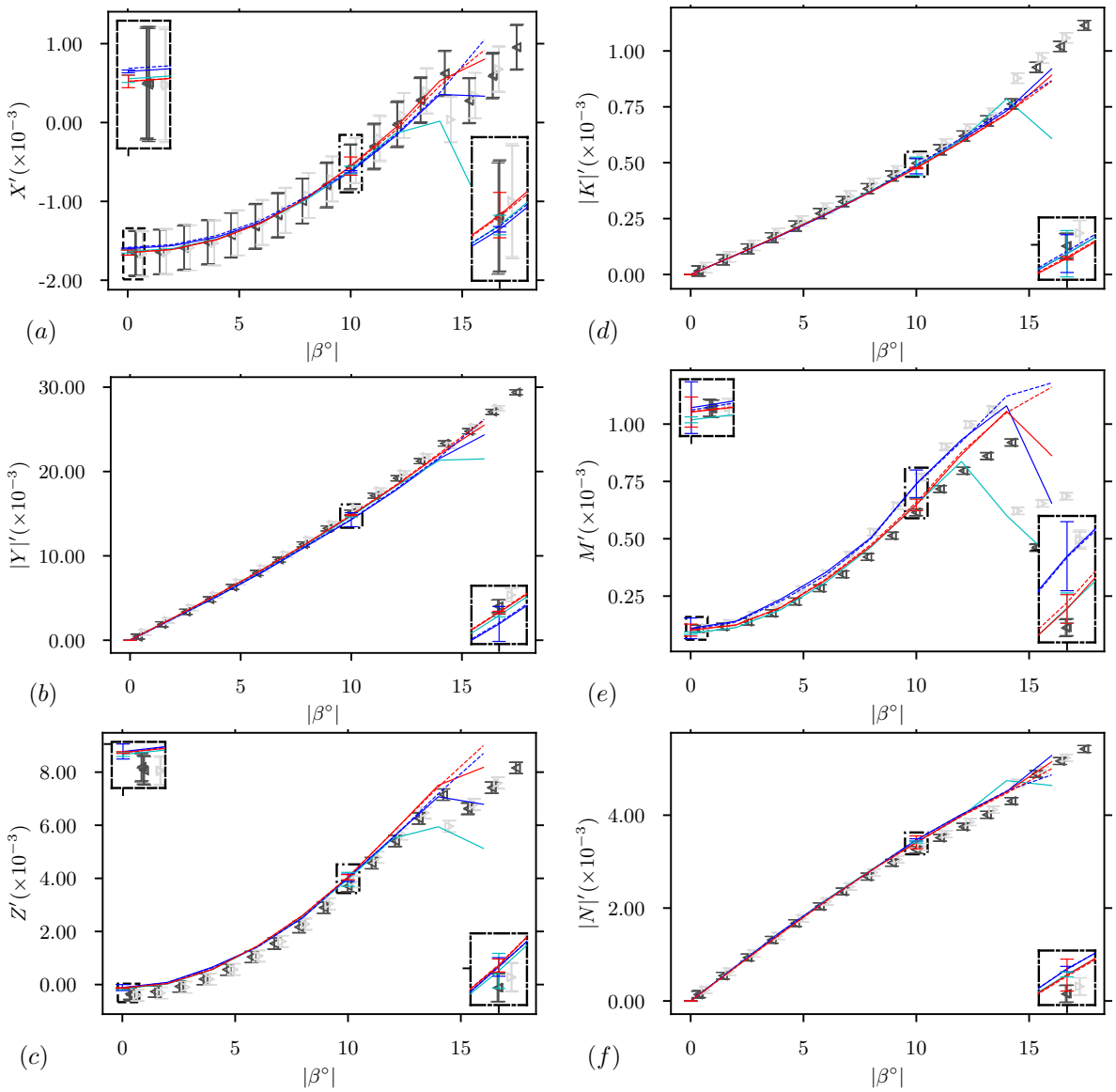

Figure 3: Experimental and RANS predicted loads for the BB2 model in the DST LSWT for a range of drift angles, $\mathrm{Re}_L = 8 \times 10^6$. Load coefficients are: (*a*) Surge force; (*b*) Sway force; (*c*) Heave force; (*d*) Roll moment; (*e*) Pitching moment; (*f*) Yaw moment. Insert boxes at $\beta = 0°$ and 10° have a zoom factor of 2.5. Lines and markers are: LSWT $-\beta$, ⊟ ;LSWT $+\beta$, ⊞ ; SST $k\omega$, ——; SST $k\omega$ CC, - - - -; BSL-RSM, ——; $k\varepsilon$ Realizable, ——; $k\varepsilon$ Realizable CC, - - - -.

models and the $k\varepsilon$ realizable model is minimal.

Discussion

Consistent with previous studies, the BSL-RSM performs better on an axisymmetric submarine geometry compared to the other turbulence models evaluated. However, with the addition of appendages, it does not have better agreement with experiment.

The large change in the predicted windward-lower-ACS stall with turbulence model, and the predicted stall of the sail by the BSL-RSM model, indicates difficulty predicting appendage lift at high incidence angles. Visualisation of skin-friction lines from the RANS solutions shows the stall originates from a corner flow separation at the appendage/hull junction. Corner flow separation might be of more significance to submarines when compared to applications such as aircraft, due to the relatively thick boundary layers compared to appendage span.

For the appended BB2, the largest difference between turbulence models prior to stall is seen in the pitching moment, figure 3(*e*). An analysis of the loads on each individual appendage reveals the leeward sail hydroplane contributes a surprisingly significant amount of this difference. Figure 5 shows the pitching moment with the leewards sail hydroplane contribution removed. Up to stall, the agreement between turbulence models is good. Removal of the leeward sail hydroplane contribution does not have a significant effect on the submarine heave force. While the cause of the pitching moment difference in the CFD is due to turbulence modeling, it does suggest the drift angle sensitivity of the experiment could also be partially due to the leeward sail hydroplane, possibly due to flow non-uniformity in the LSWT. However, flow non-uniformity would affect the non-axisymmetric hull and all appendages.

The similar prediction of heave force by all turbulence models, and pitching moment when ignoring the leeward hydroplane, indicates the sail vortex and hull interaction was not significantly affected by the turbulence model with the grid resolution used. On coarser grids, different turbulence models might predict differing vortex decay, creating a heave force and pitching

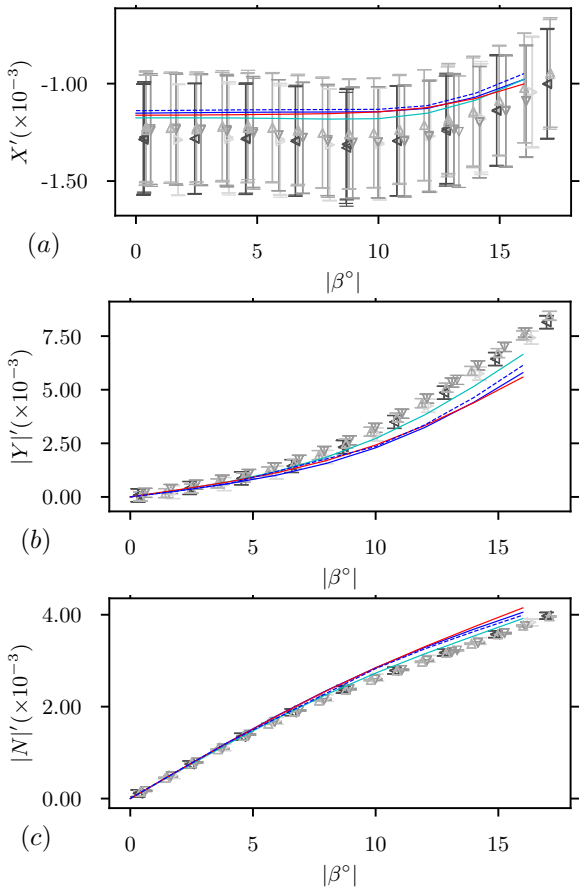

Figure 4: Experimental and RANS predicted loads for the unappended (axisymmetric) BB2 model in the DST LSWT for a range of drift angles, $\mathrm{Re}_L = 8 \times 10^6$. Load coefficients are: (*a*) Surge force; (*b*) Sway force; (*c*) Yaw moment. Lines and markers are: LSWT $-\beta$, ;LSWT $+\beta$, ; LSWT $-\alpha$, ; LSWT $+\alpha$, SST $k\omega$,;——; SST $k\omega$ CC, ------; BSL-RSM, ——; $k\varepsilon$ Realizable, ——.

moment dependency on the turbulence model.

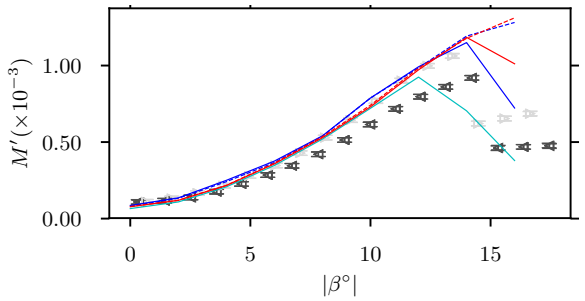

Figure 5: RANS loads for the appended BB2 model with the leeward sail hydroplane contribution removed. Experimental loads are not modified. Lines and markers are: LSWT $-\beta$, ;LSWT $+\beta$, ; SST $k\omega$, ——; SST $k\omega$ CC, ------; BSL-RSM, ——; $k\varepsilon$ Realizable, ——;$k\varepsilon$ Realizable CC,------.

Conclusion

For the appended BB2, the loads predicted by the RANS turbulence models evaluated were good up to a drift angle of approximately 10°. The exception was the pitching moment due to an experimental dependency on drift angle direction, and sensitivity of the leeward hydroplane contribution with RANS turbulence model. Prediction of appendage stall was also significantly affected by turbulence model choice, with the BSL-RSM predicting stall at a lower drift angle than the experiment, and the two-equation models with curvature correction not predicting stall in the examined drift angle range. It can be concluded that the BSL-RSM model, and the two-equation models with curvature correction, did not improve load prediction relative to the two-equation turbulence models (SST $k\omega$ or $k\varepsilon$ Realizable). However, for an unappended BB2 model, the BSL-RSM model did predict loads in closer agreement with the experiment.

References

[1] Bettle, M., *Unsteady Computational Fluid Dynamics Simulations of Six Degrees-of-Freedom Submarine Manoeuvres*, Ph.D. thesis, University of New Brunswick, 2012.

[2] Bridges, D., Blanton, J., Brewer, W. and Park, J., Experimental Investigation of the Flow past a Submarine at Angle of Drift, *AIAA Journal*, **41**.

[3] Eça, L. and Hoekstra, M., A procedure for the estimation of the numerical uncertainty of CFD calculations based on grid refinement studies, *Journal of Computational Physics*, **262**, 2014, 104 – 130.

[4] Erm, L., Calibration of the Flow in the Test Section of the Low-Speed Wind Tunnel at DSTO, Technical Report DSTO-TR-1384, Defence Science & Technology Organisation, 2003.

[5] Gerasimov, A., How to Make the Second-Moment Turbulence Closure (Reynolds-Stress Models, RSM) Work?, Technical report, ANSYS Sweden AB, 2014.

[6] Jeans, T. L., Watt, G. D., Gerber, A. G., Holloway, A. G. L. and Bake, C. R., High-Resolution Reynolds-Averaged Navier–Stokes Flow Predictions over Axisymmetric Bodies with Tapered Tails, *AIAA Journal*, **47**, 2009, 19–32.

[7] Jones, M., Quick, H. and Lam, S., Japan/Australia Joint Hydrodynamics Research: Force, moment and surface pressure results for BB2 model tested in a wind tunnel, Manuscript in preparation, Defence Science & Technology Group, 2018.

[8] Leong, Z. Q., Ranmuthugala, D., Penesis, I. and Nguyen, H. D., RANS-based CFD prediction of the hydrodynamic coefficients of DARPA SUBOFF geometry in straight-line and rotating arm manoeuvres, *Int. J. Marit. Eng.*, **154**.

[9] MARIN, BB2 Dataset, http://www.marin.nl/web/ships-structures/navy/submarines.htm.

[10] Overpelt, B., Nienhuis, B. and Anderson, B., Free Running Manoeuvring Model Tests on a Modern Generic SSK Class Submarine (BB2), in *Pacific International Maritime Conference*, Sydney, Australia, 2015.

[11] Phillips, A., Turnock, S. and Furlong, M., Influence of turbulence closure models on the vortical flow field around a submarine body undergoing steady drift, *J Mar Sci Technolo*, **15**, 2010, 201–217.

[12] Watt, G., ANSYS CFX–10 RANS Normal Force Predictions for the Series 58 Model 4621 Unappended Axisymmetric Submarine Hull in Translation, Technical Report TM 2006–037, Defence R&D Canada – Atlantic, 2006.

[13] Watt, G., Tanguay, B. and Cooper, K., Submarine hydrodynamics in the wind tunnel: The DREA Static Test Rig, in *RINA Warship 91 International Symposium on Naval Submarines 3*, London, England, 1991.